1   **A quantitative proteomic approach for unveiling novel mechanisms associated to**

2   **MeHg-induced toxicity: Effects on the methylation cycle**

3

4

5   Pablo Cabezas-Sanchez, Estefania Garcia-Calvo, Carmen Camara, Jose L. Luque-Garcia*

6   Department of Analytical Chemistry. Faculty of Chemistry. Complutense University of Madrid. 28040,

7   Madrid, Spain

8   *Address correspondence to jlluque@quim.ucm.es Tel. +34913944318

9

10   **Abstract**

11

12   Methylmercury (MeHg) is still a major threat for human health and the environment due to its

13   extremely high toxicity that mainly affects the nervous system. Despite the great efforts carried out

14   during the last decades, the specific molecular mechanisms involved in MeHg-induced toxicity are still

15   not completely unveiled. In this work we explored such mechanisms using neuroblastoma cells (Neuro-

16   2a) and SILAC as quantitative proteomic approach. We found that exposure of Neuro-2a cells to 2 mg

17   L^{-1} MeHg for 8 h decreased the cell viability to a 70% and caused significant changes in the

18   morphology of the cells, specially regarding neurites development. Our proteomic results showed

19   different proteins altered upon MeHg exposure that helped to identify pathways related to the toxicity

20   exerted by MeHg. Specifically, we have found that MeHg affect the methylation cycle by inhibiting the

21   expression of key enzymes including MTHFD1 and MTR. Moreover, we demonstrate that inhibition of

22   MTHFD1 is not observed when exposing the cells to inorganic Hg and other heavy metals such as Pb

23   or Cu. Thus, this work set the stage for dissecting a specific molecular mechanism for MeHg-induced

24   toxicity.

25

26

27

28

29

30   **Key words**: Methylmercury toxicity, methylation cycle enzymes, SILAC, quantitative proteomics

31

Introduction

33

34   Mercury is one of the most hazardous environmental pollutants representing a serious risk to human

35   health. It can be easily methylated by widespread sulfate-reducing bacteria into methylmercury (MeHg),

36   which easily penetrates into organisms through the lipid bilayer.[1] As a result of this biomethylation,

37   MeHg distributes among tissues, being the central nervous system the most sensitive target organ.[2] It is

38   also known that ingested mercury can interact with some proteins and enzymes causing organ

39   dysfunction.[3] Some neurotoxic effects such as mental retardation, dysmorphogenesis of the cerebellum,

40   degeneration of granule cells, neurons or dorsal root ganglia have been observed in episodes of

41   mercury poisoning.[4] Extensive research has been conducted to determine the molecular mechanisms

42   associated to MeHg uptake and neurotoxicity. It has been suggested that MeHg entered in neural cells

43   as a cysteine complex via the L-type neutral amino acid carrier transport (LAT) system due to the

44   similitude between this complex and L-methionine, a substrate for the amino acid transport system.[5] It

45   is also known that MeHg inhibits several mitochondrial enzymes such as glutathione peroxidase,

46   glutathione reductase[6] and the thioredoxin system,[7] and induces apoptosis and necrosis in neural

47   cells.[8,9] However, despite all the efforts conducted over the last half century, identification of particular

48   biomolecular mechanisms underlying the observed neurotoxic effects of MeHg have not yet been

49   proposed.[10]

50   With the advent of biological mass spectrometry, novel proteomic strategies have been

51   applied to investigate toxicity mechanisms.[11] Specifically, quantitative proteomics allows for the

52   identification of differentially expressed proteins between two or more different physiological

53   conditions, thus contributing to the discovery of candidate toxicity-specific targets and molecular

54   pathways. Stable isotopic labeling by amino acids in cell culture (SILAC) is one of the most widely

55   used alternatives for relative protein quantitation due to its high accuracy and because it offers the

56   possibility for the identification and quantitation of proteins within the same experiment.[12,13] SILAC

57   involves the addition of ^{12}C- and ^{13}C-labeled lysine and arginine to growth media of separately cultured

58   cells, giving rise to cells containing "light" or "heavy" proteins, respectively.

59   In this work, we have used the SILAC approach as a discovery platform for the identification

60   of 125 proteins affected by MeHg exposure. The combination of this quantitative proteomic strategy

61   with additional bioanalytical assays has allowed for the identification of mechanisms related to MeHg

62   toxicity and to set the stage for dissecting a specific molecular mechanism in which the methylation

63   cycle blockage upon MeHg exposure is involved.

64

65   **Materials and methods**

66   **Cell culture and cytotoxicity assay**

67   Mouse neuroblastoma cells (Neuro-2a) were maintained in Dulbecco´s Modified Eagle Medium

68   (DMEM) supplemented with 10% fetal bovine serum (FBS) and 100 units/ml of

69   penicillin/streptomycin in 5% CO_2 at 37ºC. 2×10^4 cells were plated onto 96-well plates and incubated

70   with methylmercury (MeHg) at different exposure times. Cell viability was determined using the MTT

71   assay. 20 µL of MTT (5 mg L^{-1}) were added to each well and incubated during 5 h. After this time, the

72   MTT solution was removed and 100 µL of dimethyl sulfoxide (DMSO) were added to dissolve the

73   insoluble purple formazan product. Cell viability was quantified by measuring the absorbance at 595

74   nm in a microplate absorbance reader (Sunrise, Tecan). The same procedure was used for measuring

75   the viability when exposing the cells to the combination MeHg-vitamin B12, and for cells transfected

76   with siRNA against MTHFD1.

77

78   **Determination of MeHg uptaked by Neuro-2a cells**

79   After exposing 1×10^7 cells to 2 mg L^{-1} MeHg for 8 h, the exposure medium was removed and reserved,

80   and the cells were thoroughly washed with PBS and collected. Samples were digested in a microwave

81   oven with a mixture of HNO_3 (65%) and H_2O_2 (35%). Digested samples were introduced in a flow

82   injection system where mercury was reduced to atomic mercury vapor with 3% stannous chloride.

83   Determination of total mercury in both, the exposure media and the cells was carried out by cold vapor

84   atomic fluorescence spectroscopy (CV-AFS) (Merlin 10.023). All samples were analyzed in

85   quadruplicate. Certificated reference materials from the Commission of the European Communities

86   (CRM) were also analyzed to ensure the quality of the results. Recoveries from CRM-029 and CRM-

87   710 were within 5% of the certificated values. Calculated limits of detection (LOD) and quantification

88   (LOQ) were 6 ng L^{-1} and 23 ng L^{-1}, respectively.

89

90   **Evaluation of morphological changes**

91   Cells (2 x 10^6 cells) were seeded onto coverslips 48 h before MeHg exposure in order to reach 80 %

92   confluence. At this point, cell viability was checked and no significant decrease was observed. Cells

93   were incubated with MeHg 2 mg L^{-1} for 8 h and then washed with ice-cold PBS, fixed with

94   paraformaldehyde (4% v/v) for 15 min at room temperature and permeabilized with 5 ml of Triton X-

95   100 (0.1% v/v, 40 mM glycine). Cells were then incubated with Alexa Fluor 488-labeled phalloidine

96   (1:60) for 20 min at room temperature. Staining of nuclei was performed in a 1 mg mL^{-1} solution of

97   4′,6-diamino-2-phenylindole (DAPI) and finally, coverslips were mounted with Mowiol® 4-88.

98   Fluorescence microscopy was performed in a Motic AE31 epifluorescence microscope and

99   representative images were acquired with a 60x objective using the Motic Images Advanced 3.2

100 Software.

101

102 **SILAC protein profiling**

103 Neuro-2a cells were maintained in DMEM medium supplemented with 10 % dialyzed FBS, 100

104 units/ml of penicillin/streptomycin and either naturally-occurring isotope abundances ("light") or stable

105 isotope-labeled ("heavy") $^{13}C_6$ arginine and $^{13}C_6$ lysine amino acids. Culture media were refreshed

106 every 2 days and cells were grown for at least 6 doublings to allow full incorporation of labeled amino

107 acids. Two large-scale SILAC replicates (1 x 10^7 cells per condition) were performed. Complete

108 incorporation of ^{13}C-Arg and ^{13}C-Lys into control and MeHg-exposed Neuro-2a cells after 6 cell

109 divisions in isotopically heavy medium (direct and reverse SILAC, respectively) was verified by MS

110 analysis of a protein digest (data not shown).

111   After differential labeling, control and cells exposed to 2 mg L^{-1} MeHg for 8 h were mixed in

112 a 1:1 ratio. Cell lysates were prepared in RIPA buffer containing protease inhibitor cocktail (Roche).

113 Protein extracts were separated by SDS-PAGE on 10% SDS-polyacrylamide gels, visualized by

114 Coommassie blue staining and the gel lanes were cut horizontally into 20 sections. Excised gel bands

115 were de-stained in 50:50 25 mM ammonium bicarbonate/acetonitrile and dried. Gel pieces were

116 rehydrated with 12.5 ng $μL^{-1}$ trypsin solution in 25 mM ammonium bicarbonate and incubated

117 overnight at 37ºC. Peptides were extracted using acetonitrile and 5% formic acid, dried by vacuum

118 centrifugation and reconstituted in 10 μL 2% acetonitrile in 0.1% formic acid.

119   The peptide mixtures from in-gel digestions were analyzed using nanoflow LC-MS/MS

120 (Eksigent). Peptides were loaded onto a 0.3 x 10 mm C18 precolumn (SGE) and separated on a

121   reverse-phase column (75 μm x 15 cm fused silica capillary C18 HPLC PepMap column, 3 μm , 100 A,

122   Thermo) with linear gradient of 5-95% acetonitrile in 0.1 % aqueous solution of formic acid. The

123   samples were delivered over 120 min at a flow-rate of 200 nL min^{-1} through the analytical column to a

124   stainless steel nano-bore emitter (Proxeon). The peptides were scanned and fragmented with an LTQ

125   XL linear ion trap mass spectrometer (Thermo Scientific) operated in data-dependent ZoomScan and

126   MS/MS switching mode using the three most intense precursors detected in a survey scan from 400 to

127   1600 u (three μscans). ZoomScan mass widow was set to 12 Da enabling monitoring of the entire

128    $^{12}C/^{13}C$ isotopic envelope of most doubly and triply charged peptides. Singly charged ions were

129   excluded for MS/MS analysis. Normalized collision energy was set to 35% and dynamic exclusion was

130   applied during 3 min periods to avoid repetitive fragmentation ions.

131   Generated .raw files were converted to .mgf files for MASCOT data search. A database

132   containing the NCBInr Mouse sequences containing 34966 entries (as of 10-09-14) was searched using

133   MASCOT Software (version 2.3 MatrixScience) for protein identification. Oxidation of methionine

134   and $^{13}C_6$-Arg and $^{13}C_6$-Lys were specified as variable modifications, trypsin as specific enzyme and one

135   missed cleavage allowed. Minimum precursor and fragment-ion mass accuracies for 1.2 and 0.3 Da

136   were used. A requirement of at least one bold (unique) red peptide (i.e. highest scoring peptide

137   matching to protein with highest total score) was required for protein identification and at least two

138   bold red (unique) peptides were required for quantification. Cut-off values for MASCOT scores of

139   peptides and proteins were set to 38 (*p<0.05*) and 45 (*p<0.01*), respectively. The false positive rate was

140   calculated by searching the same spectra against the NCBInr Mouse decoy database. Relative

141   quantitation ratios of identified proteins were calculated using QuiXoT (version 1.3.26). SILAC ratios

142   were defined by the area of the heavy peptides (^{13}C) divided by the area of light peptides (^{12}C). Protein

143   ratios obtained by QuiXot were manually verified for all peptides. As observed in previous studies, a

144   proportion of $^{13}C_6$-Arg was converted to $^{13}C_5$-Pro leading to a reduction in the intensity of the isotope-

145   labeled peptide peak; this was corrected for all peptides containing one or more proline residues by

146   adding the intensity found for the peptide containing $^{13}C_6$-Arg$^{13}C_5$-Pro or $^{13}C_6$-Lys$^{13}C_5$-Pro to the

147   intensity of the peak containing only $^{13}C_6$-Arg or $^{13}C_6$-Lys. Molecular and cellular functions of the

148   proteins found de-regulated by SILAC were assigned based on the biological knowledge available in

149   Gene Ontology (GO) annotations.

150

151 **Western blotting**

152 Total protein content was extracted from Neuro-2a cells using RIPA lysis buffer and quantified with

153 the Bradford assay using BSA as standard. Total protein extracts were separated on 7.5% SDS-

154 polyacrylamide gels and electrotransferred to nitrocellulose membranes (BioRad). Membranes were

155 blocked with 3% skim dry milk in PBS-T (0.05 % Tween-20) for 1 h at room temperature and

156 incubated overnight at 4ºC with primary antibodies against: Methylenetetrahydrofolate dehydrogenase

157 1 (MTHFD1) (1:500, Santa Cruz), methionine synthase (MTR) (1:1000, Sigma-Aldrich) and

158 glyceraldehyde 3-phosphate dehydrogenase (GAPDH) (1:10000, Sigma-Aldrich). The blots were

159 washed in PBS-T and incubated with horseradish peroxidase-conjugated secondary antibodies for 1 h

160 at room temperature. Antibody binding was visualized using enhanced chemiluminescent

161 immunoblotting detection system (GE Healthcare).

162

163 **MTHFD1 gene knock-down**

164 Knock-down of MTHFD1 was performed by transient transfection with Lipofectamine and reduced

165 serum media (Opti-MEM) using control (not-targeting) small interfering doubled-stranded RNA

166 (siRNA) and siRNA targeted against MTHFD1. MTHFD1 silencing transfectants exposed to 10 and 30

167 pmoL of targeted siRNA were collected at 24 h for MTT assay as described above. MTFHD1 silencing

168 was confirmed by immunoblotting.

169

170 **Results and discussion**

171 **Cytotoxicity, mercury uptake and morphological changes induced by MeHg exposure**

172 We evaluated the cytotoxicity induced by MeHg in Neuro-2a cells using the MTT assay that measures

173 the reducing potential of cells; while viable cells are able to reduce the MTT to formazan (a purple

174 compound), non-viable cells are unable to do so. We selected concentrations of MeHg ranging from

175 0.5 to 5 mg L^{-1} and exposure times between 6 and 24 h. The viability of cells exposed to 0.5 mg L^{-1}

176 MeHg was not affected at the exposure times tested (see Fig. 1a). However, the highest concentration

177 assayed (5 mg L^{-1}) caused a decrease on the cell viability close to 100% even after 6 h of exposure. On

178 the other hand, the viability of Neuro-2a cells exposed to 2 mg L^{-1} MeHg decreased on a time-

179 dependent manner. It is important to mention that since MeHg was dissolved in MeOH, we tested the

180 potential effect of MeOH on the cell viability, and no significant changes were observed as compared

181   to control cells (data not shown). This data is in accordance with a previous report in which HepG2

182   cells were exposed to MeHg. Cell viability of HepG2 cells diminished to practically the same extent at

183   the same MeHg concentrations and exposure times tested[13] as Neuro-2a cells. In order to evaluate the

184   effect of MeHg in Neuro-2a cells but without drastically compromising the cell viability, we selected 2

185   mg L^{-1} and 8 h as exposure time for further experiments.

186   We also evaluated morphological changes induced after MeHg exposure by fluorescence

187   microscopy. Neuro-2a cells were allowed to extend neurites for 48 h before exposure to 2 mg L^{-1}

188   MeHg for 8 h. Exposure to MeHg markedly disrupted the structural integrity of neurites (see Fig. 1b).

189   We finally determined the total amount of MeHg internalized by the cells by atomic

190   fluorescence spectroscopy (AFS). Our results (see Fig. 1c) showed that a 10% of the total MeHg added

191   were actually found inside the cells. These results reflect that the amount of internalized MeHg can

192   significantly impair cell viability, functioning and morphology.

193

194   **Differential protein expression of Neuro-2a cells exposed to MeHg**

195   In order to identify novel molecular pathways related to MeHg toxicity, we have used a state-of-the-art

196   quantitative proteomic approach (SILAC) able to quantify differentially expressed proteins in MeHg-

197   exposed cells as compared to control Neuro-2a cells. In our SILAC experiment, we carried out two

198   large-SILAC experiments. We identified a total of 1524 proteins (see Fig. 2a), from which 978 proteins

199   passed the criteria established for protein quantitation. Most of the quantified proteins presented a

200   SILAC ratio close to 1, as expected for a 1:1 mixture (see Fig. 2b). The overall false discovery rate was

201   1.3% being estimated by the number of hits against the reverse sequence/total hits (p<0.01). The mean

202   relative standard deviation (RSD) of the ratios obtained from replicates was lower than 20%, indicating

203   good agreement between experiments. Using 1.5 as the threshold ratio, we found 125 proteins altered,

204   48 of which were over-expressed (Table 1) and 77 down-regulated (Table 2) upon MeHg exposure.

205   The full list of proteins identified in both replicates using SILAC is in Supplementary Table 1.

206   The functional annotation of the 125 altered proteins upon MeHg exposure were obtained

207   from the gene ontology GO consortium website. Major molecular and cellular functions altered

208   included cell death, RNA post-transcriptional modification, protein synthesis, cellular assembly and

209   organization, and cell cycle (see Fig. 2c). We also looked for the molecular pathways in which altered

210   proteins might play key roles. Such pathways included apoptosis (PIR, CDK1, CAD, MO25, BAX,

211   CEND1, CUL3, BCL2A1, COP9), stress resistance (MCM5, MCM2, ALDH2, TRX, TRXR1), ROS

212   generation (NDUFS3, GST), axonogenesis (IPO9, TUBB2B, MSN, DYN) and neurodegeneration

213   (RAB1B, COPE). Alteration or activation of some of these mechanisms has already been associated

214   with MeHg toxicity.

215

216   **MeHg induces cell death through the intrinsic and extrinsic apoptotic pathways**

217   Several previous reports have demonstrated how MeHg exposure activates the apoptotic pathway in

218   different cell cultures and animals.[8,13–15] Apoptosis is a naturally occurring process by which a cell is

219   directed to programmed cell death. It involves the activation of caspases, a family of cysteine proteases,

220   and a complex cascade of events that link the initiating stimuli to the final demise of the cell.[16]

221   Activation of caspases can be initiated at the plasma membrane upon ligation of death receptor

222   (extrinsic pathway) or at the mitochondria induced by intracellular stress (intrinsic pathway). Most

223   previous studies on MeHg toxicity have demonstrated the activation of the apoptotic intrinsic pathway

224   and thus, alteration of the expression of well-known apoptotic markers such as the caspases and the

225   Bcl2 protein family after MeHg exposure.[17] In agreement with these studies, we have also found

226   alteration of some of these proteins, thus suggesting MeHg-mediated activation of the apoptotic

227   intrinsic pathway. We show overexpression of the pro-apoptotic protein BAX ($R_{SILAC} = 2.52$) and

228   inhibition of anti-apoptotic proteins BCL2A1 ($R_{SILAC} = -1.64$) and BAG3 ($R_{SILAC} = -1.81$), in Neuro-2a

229   cells exposed to MeHg. While BAX induces opening of the mitochondrial voltage-dependent anion

230   channel (VDAC) resulting in the release of cytochrome c and other pro-apoptotic factors, BCL2A1

231   have the opposite role by reducing the release of pro-apoptotic cytochrome c and blocking caspase

232   activation. BAG3 is a modulator of cellular anti-apoptotic activity that functions through its interaction

233   with Bcl-2.[18–20] We also found significant overexpression of CAD ($R_{SILAC} = 2.92$), which is activated

234   by caspase 3 and causes DNA degradation in the nucleus of apoptotic cells. Besides these well-known

235   apoptotic markers, our SILAC approach has allowed us to find additional routes that are also being

236   activated by MeHg and thus, should be considered for a better understanding of the mechanisms related

237   to MeHg-induced cell death.

238   The ubiquitin-proteasome system (UPS) constitutes a major degradation pathway for

239   intracellular proteins and plays an important role regulating apoptosis. In this pathway, proteins, which

240   are going to be degraded by the proteasome, are first tagged with a polypeptide called ubiquitin (Ub) in

241 order to be later recognized and degraded by the 26S proteasome. Ubiquitination reaction is carried out

242 by a set of enzymes called ubiquitin ligases or E3s, which transfer the ubiquitin moiety to the

243 substrate.[21] Within this molecular machinery, there is an essential family of proteins named cullins,

244 which provide a scaffold for ubiquitin ligases. These proteins combined with RING proteins form the

245 Cullin-RING ubiquitin ligases (CRLs) that contain the catalytic core needed for the ubiquitination

246 reaction. In our experiment, we have found overexpression of CUL3 (R_{SILAC} = 1.88) in Neuro-2a cells

247 exposed to MeHg. CUL3, which is one of the four members of the cullin protein family,[22] mediates the

248 ubiquitination of caspase-8.[23] Overexpression of CUL3 might increase aggregation of CUL3-modified

249 caspase-8, thus inducing full activation and processing of caspase-8 and thereby, leading to robust

250 stimulation of effector caspases and apoptosis.[24] It is also important to consider the interplay between

251 Ub family modifiers that creates a regulatory network with the Ub family proteins. One of the best-

252 studied crosstalks between Ub family modifiers is the stimulation of ubiquitination by Nedd8 (neural

253 precursor cell expressed developmentally down regulated 8) modification. Neddylation of the cullin

254 scaffolds of the CRLs, allosterically activates the transfer of Ub from the CRLs to the target

255 substrates.[25] The neddylation-deneddylation pathway of the CRLs is regulated by the COP9

256 signalosome (CSN). CSN has an intrinsic metalloproteinase that removes the Nedd8 from cullins

257 (deneddylation), thus converting CRLs into an inactive state.[25] Interestingly, COP9 is downregulated in

258 our experiment (R_{SILAC} = -3.45), this deficiency of COP9 induced by MeHg exposure might preclude

259 deneddylation of the CRLs, also promoting ubiquitination of caspase-8 by CUL3 and therefore, the

260 apoptotic pathway. These results are in agreement with a recent report demonstrating that deficiency of

261 COP9 induces ubiquitin-proteasome system impairment and apoptosis.[26] Although previous reports

262 support the idea that MeHg-induced apoptosis occurs through activation of the intrinsic apoptotic

263 pathway;[13,27] taken together, our results suggest that MeHg could induce apoptosis through both

264 extrinsic and intrinsic pathways in Neuro-2a cells.

265   Considering the link between cell cycle and apoptosis, it is not surprising that some of the

266 proteins we found affected by MeHg exposure are related with cell cycle regulation. CDK1, also

267 known as CDC2, is a serine/threonine protein kinase that plays a well-characterized role in cell cycle

268 control and cellular differentiation. CDK1 is critical for G2/M transition and mitosis. Several studies

269 have demonstrated the relevant role of CDK1 in some forms of apoptosis.[28] It has been shown that

270 CDK1-mediated phosphorylation of BCL2 family proteins enhances their pro-apoptotic function.[29]

271 Thus, the overexpression of CDK1 (R_{SILAC} = 2.80) in cells exposed to MeHg, might explain the

272 significant overexpression of pro-apoptotic proteins observed in our SILAC experiment. We have

273 found a similar degree of overexpresion for CEND1 (R_{SILAC} = 2.10), which is a neuronal-lineage

274 specific regulator that coordinates cell cycle withdrawal and differentiation of neuronal progenitors. It

275 is involved in histone deacetylase inhibition-mediated growth arrest of neuroblastoma cells,[30] and its

276 overexpression in fibroblasts has been shown to trigger cell cycle exit, droving cells towards a pro-

277 apoptotic pathway.[31]

278   We have also found two additional proteins highly upregulated, MO25 (R_{SILAC} = 2.68) and

279 PIR (R_{SILAC} = 2.98), whose overexpression have been previously associated to a higher degree of

280 apoptosis. MO25 is a scaffold protein that can directly interact with certain STE20 kinases including

281 MST4 (mammalian STE20-like kinase) increasing its kinase activity.[32] MST4 regulates multiple

282 cellular aspects such as cell polarity and proliferation. In fact, MST4 might be one of the targets for

283 caspase 3.[33] It has been demonstrated that overexpression of MO25 activates MST4 resulting in

284 dramatically increased apoptosis.[34] PIR is an iron-binding nuclear protein and transcription cofactor

285 that stabilizes the formation of quaternary complexes between Bcl-3, NF-kB and a DNA target protein

286 directing the NF-kB DNA binding towards a pro-apoptotic response.[35] Overexpression of PIR has been

287 associated with an increased apoptosis in several cellular types.[35,36]

288

289 **MeHg induces overexpression of proteins involved in ROS generation and stress resistance**

290   MeHg is considered to increase reactive oxygen species (ROS) generation, thus inducing an

291 imbalance in the normal redox state of cells, which results in damaging of cell components and

292 structures.[37] Since this process, known as oxidative stress, is directly related with apoptosis, we

293 expected to find some proteins involved in ROS generation, oxidative stress and stress resistance, up-

294 or down-regulated upon MeHg exposure. Actually, we found overexpression of NDUFS3 ((R_{SILAC} =

295 2.65) and downregulation of GST (R_{SILAC} = -1.74). NDUFS3 is a subunit of the NADH:ubiquinone

296 oxidoreductase ETC complex I involved in electron transfer and coupling.[38] Overexpression of

297 NDUFS3 has been previously related to ROS generation and apoptosis.[39,40] GST is a well-known

298 antioxidant enzyme and its inhibition markedly exaggerates oxidative-stress induced apoptosis.[41] In

299 addition, it has also been demonstrated that GST inhibition is associated with increased activation of

300 MAP kinases, a family of proteins that play crucial roles in stress response, cell survival and

301   apoptosis.[42] We also found overexpression of several antioxidant proteins such as TRXR1

302   (R_{SILAC}=2.23) and TRX (R_{SILAC}=1.99), which upregulated or overexpressed, protect against oxidative

303   stress. Upregulation of these proteins show a defense mechanism against MeHg-induced toxicity based

304   on the disulfide reductase activity of TRX, and thereby on the supply of NADPH and the activity of

305   TRXR1.[43] Upregulation of ALDH2 (R_{SILAC}=2.93) show an additional defense mechanism since

306   ALDHs metabolize endogenous and exogenous aldehydes and thereby mitigate oxidative stress in

307   prokaryotic and eukaryotic organisms.[44] In the case of minochromosome maintenance proteins

308   (MCMs), which are required for DNA replication in eukaryotic cells, their expression is restricted to

309   proliferating and dedifferentiated tissues and is a typical feature of many malignant and premalignant

310   diseases. Overexpression of MCM is one of the molecular determinants of highly mitogenic

311   phenotypes.[45] Thus, we could have expected downregulation of these proteins since Neuro-2a cells

312   exposed to MeHg undergo apoptosis. However, we found upregulation of two MCM proteins (MCM5,

313   R_{SILAC}= 3.71; MCM2, R_{SILAC}= 1.85) what can be explained as an additional cellular defense

314   mechanism against MeHg toxicity, since it has been demonstrated that overexpression of MCM is

315   needed for cells to withstand stress conditions.[46]

316

317   **MeHg exposure affects neurites integrity and development**

318   Our evaluation of morphological changes in Neuro-2a cells after exposure to MeHg demonstrates a

319   significant disruption of the structural integrity of neurites, which are precursors of either axons or

320   dendrites (see Fig. 1b). In relation with this observation, we found significantly inhibited several

321   proteins related to axonogenesis, neurite outgrowth and microtubule formation. While IPO is

322   constitutively complexed with the retrograde motor DYN, being the DYN-IPO complex essential for

323   axonogenesis,[47] the complex DYN-CTTN plays a central structural role in focal adhesion assembly in

324   neuronal growth cone.[48] In our SILAC experiment, we found not only down-regulation of DYN

325   (R_{SILAC}= -1.68), which is in agreement with a previous study that demonstrated that a reduction in

326   DYN prevented neurite formation in cultured hippocampal neurons;[49] but also IPO (R_{SILAC}= -2.24) and

327   CTTN (R_{SILAC}= -3.84), which form key complexes with DYN as commented before, also appeared

328   downregulated, showing a significant damage induced by MeHg on axonogenesis. We observed a

329   similar down-regulation in the case of MSN (R_{SILAC}= -1.72), which plays a key role in generating and

330   maintaining the normal structure and functional organization of neuronal growth cones.[50] In addition,

331   we found downregulated other proteins directly related to neurite extension such as tubulins (TUBB2B,

332   R_{SILAC}= -4.48; TUBA1C, R_{SILAC}= -1.83), whose assembly is essential for microtubule formation and

333   thus, for neurite extension; and kinesins (KIF5C, R_{SILAC}= -18.73; KIF11, R_{SILAC}= -2.41), which have

334   been recently recognize as microtubule motors providing the mechanical forces necessary for initial

335   neurite extension.[51] Altogether, these findings are consistent with earlier evidences demonstrating that

336   microtubule metabolism is compromised in the presence of Hg ions,[52] and confirm how MeHg directly

337   affect development of neurites, therefore demonstrating the detrimental effect of MeHg on

338   axonogenesis.

339

340   **MeHg induces blockage of the methylation cycle mediated by downregulation of MTHFD1 and**

341   **MTR**

342   One of the down-regulated proteins that we found particularly interesting in our SILAC experiment is

343   the enzyme methylenetetrahydrofolate dehydrogenase 1 (MTHFD1) (R_{SILAC}= -1.67), which plays a key

344   role in the methylation cycle. This cycle is the principal mechanism whereby vitamin B12 and folate

345   metabolism influence in brain function and to DNA methylation, synthesis and repair. Folate

346   metabolism plays a vital function for cell division and homeostasis due to the multiple enzymes[53]

347   involved in nucleic acid synthesis, methionine regeneration and reduction of carbon units required for

348   normal metabolic regulation.[54] The methylation pathway involves the conversion of homocysteine to

349   methionine where tetrahydrofolate is converted to 5,10-methylenetetrahydrofolate (5,10-MTHF) by the

350   enzyme methylenetetrahydrofolate dehydrogenase 1 (MTHFD1), followed by conversion of 5,10-

351   MTHF to 5-methyltetrahydrofolate (5-MTHF) by the methylenetetrahydrofolate reductase (MTHFR).

352   Finally, 5-MTHF reacts with homocysteine to form methionine and to regenerate tetrahydrofolate (see

353   Fig. 3). Methionine synthase (MTR) regulates this reaction, being vitamin B12 a cofactor of MTR.[55]

354   Based on these premises and a previous work[56] that correlates exposure to Hg^{2+} with inactivation of

355   MTR, we decided to further study the effect of MeHg on the methylation cycle (see Fig. 3) and,

356   particularly, on the expression of MTHFD1 and MTR. We validated the SILAC results by

357   immunoblotting (see Fig. 4), and indeed we observed a significantly decreased expression of MTHFD1

358   with increasing concentrations of MeHg. A similar behavior was observed for MTR, whose expression

359   also decreased significantly in Neuro-2a cells exposed to 2 mg L^{-1} of MeHg for 8 h as compared to

360   control cells. Inhibition of these proteins has been associated with malfunction in the synthesis,

361   methylation and reparation of DNA; thus, we hypothesize that the alteration in the expression of these

362   enzymes could be related with the mechanism of neurotoxicity activated by MeHg exposure.

363   To support our previous results, we investigated whether siRNA-mediated gene knock-down

364   of MTHFD1 induces a decrease in the cell viability of Neuro-2a cells similar to that induced by MeHg.

365   After validating the suitability of the transfection (see Fig. 5a) by Western blot, we measured the cell

366   viability in transfected cells and in cells exposed to 2 mg L^{-1} of MeHg for 8 h using the MTT assay.

367   The results show that MTHFD1 knock-down affected the viability of Neuro-2a cells, although the

368   decrease in cell viability was more pronounced in cells exposed to MeHg (see Fig. 5b). This could be

369   explained by the fact that additional mechanisms (besides the methylation cycle) are also being

370   affected by MeHg exposure.

371   Another important aspect to be considered is the fact that the methylation cycle requires

372   vitamin B12, which acts as coenzyme required for correct functioning of the methyl donation from 5-

373   methyl-THF to THF.[54] Vitamin B12 deficiency blocked the methylation cycle and induces a series of

374   pathological conditions that are quite similar to the effects induced by Hg poisoning.[57] Vitamin B12 is

375   highly reactive and vulnerable to inactivation by oxidation of the Co atom in its structure; this

376   oxidation inactivates the enzyme MTR and blocks the methylation cycle.[58] The blockage of the

377   methylation cycle causes an increase in levels of homocysteine that generates an increase concentration

378   of calcium, accumulation of reactive oxygen species (ROS), activation of MAP kinases and the release

379   of arachidonic acid from platelets that inhibits glutathione peroxidase, an antioxidant that protects cells

380   against oxidative stress.[59] Homocysteine is easy accumulated inside the cells where it undergoes

381   autoxidation transforming it into homocysteic acid accompanied by H_2O_2 accumulation.[60] In fact, a

382   long-term incubation of neurons with homocysteic acid induced necrotic cell death.[61] It is well known

383   that the effects on human health induced by Hg poisoning are very similar to those experimented by

384   individuals with a significant vitamin B12 deficiency. Several years ago, a possible hypothesis of the

385   Hg/vitamin B12 connection suggested that Hg could oxidize the Co atom in the vitamin B12, thus

386   causing denaturation of the vitamin, blockage of the methylation cycle and an increase in the levels of

387   homocysteine.[62] Although we have previously shown inhibition of MTHFD1 and MTR as the main

388   cause for the methylation cycle to be blocked upon MeHg exposure, we decided to test whether the

389   oxidation of vitamin B12 by MeHg could also be another factor to be considered. This would explain

390   why both conditions caused similar symptoms, although this hypothesis has never been experimentally

13

391   demonstrated. In order to demonstrate if another way by which MeHg affect the methylation cycle is

392   by denaturizing vitamin B12, we added increasing concentrations of vitamin B12 to Neuro-2a cells

393   exposed to MeHg. Considering the initial hypothesis, high concentrations of vitamin B12 would

394   counteract the partial oxidation of the vitamin induced by MeHg and would restore the cell viability to

395   a certain level. Our results (see Fig. 6) show that supplementation with vitamin B12 did not ameliorate

396   the decreased in cell viability observed in MeHg-exposed cells, not even at the higher concentration of

397   vitamin B12 tested.

398

399   **Comparative effect of MeHg and other heavy metals on the expression of MTHFD1 and MTR**

400   One of the challenges in toxicoproteomics is the identification of particular molecular mechanisms or

401   pathways associated to the toxicity exerted by a particular compound rather than general mechanisms

402   related to stress-response and/or cell defense.[63] To investigate whether blockage of the methylation

403   cycle mediated by downregulation of MTHFD1 and MTR could also be induced by inorganic mercury

404   or other heavy metals, we carried a comparative Western blot analysis using Neuro-2a cells exposed to

405   MeHg, Hg^{2+}, Pb^{2+} or Cu^{2+}. We selected concentrations of these ions that caused a decrease in the

406   viability of the cells similar to that induced by 2 mg L^{-1} MeHg during 8 h. Our results show that while

407   the four species highly affect the expression of MTR (see Fig. 7), the expression pattern for MTHFD1

408   was significantly different depending on the metallic species tested. Surprisingly, Hg^{2+} did not affect

409   the expression of MTHFD1, while Pb^{2+} and Cu^{2+} slightly affected the expression of this enzyme but to

410   a much lesser extent as compared to MeHg (see Fig. 7). The different behavior observed for MTHFD1

411   and MTR after exposure to these metals could explain why in a previous study, stimulation of MTR

412   with dopamine and insulin resulted in the re-activation of the methylation cycle of Neuro-2a cells

413   exposed to Cu^{2+} and Pb^{2+}, but was inefficient for cells exposed to MeHg.[57] This fact reinforces the

414   specific negative interaction found between MeHg and MTHFD1.

415

416   **Conclusion**

417   A quantitative proteomic approach (SILAC) has been used for the discovery of novel molecular

418   pathways associated to MeHg induced neurotoxicity. We have identified a set of proteins altered upon

419   MeHg exposure of Neuro-2a cells. Such altered proteins turned out to be involved in pathways related

420   to apoptosis, stress resistance, ROS generation, axonogenesis and neurodegeneration. One of the main

421   discoveries derived of our study is the MeHg-induced downregulation of key enzymes of the

422   methylation cycle (MTHFD1 and MTR). We hypothesize that the effect of MeHg blocking the

423   methylation cycle could be related with the mechanisms of neurotoxicity and the symptons observed

424   after MeHg poisoning. It could also explain the similarity observed in the symptomatology between

425   MeHg poisoning and vitamin B12 defficiency. Moreover, we have demonstrated that inhibition of

426   MTHFD1 is specific of MeHg as compared to inorganic Hg and other heavy metals such as Pb or Cu.

427   Thus, this work set the stage for dissecting a specific molecular mechanism for MeHg-induced toxicity.

428

429   **Acknowledgments**

434

435

436

437

438

439

440

441

442

443

444

445

446

447

448

449

450

451 **References**

452

453 1 V. Glaser, E. M. Nazari, Y. M. R. Müller, L. Feksa, C. M. D. Wannmacher, J. B. T. Rocha, A.

454 F. de Bem, M. Farina and A. Latini, *Int. J. Dev. Neurosci.*, 2010, **28**, 631-637.

455 2 M. Farina, J. B. T. Rocha and M. Aschner, *Life Sci.*, 2011, **89**, 555-563.

456 3 K. Eto, *Toxicol. Pathol.*, 1997, **25**, 614-623.

457 4 C. Watanabe and H. Satoh, *Environ. Heal. Perspect.*, 1996, **104**, 367-379.

458 5 L. E. Kerper, N. Ballatori and T. W. Clarkson, *Am J Physiol Regul. Integr. Comp Physiol.*,

459 1992, **262**, 761–765.

460 6 R. Dringen, *Prog. Neurobiol.*, 2000, **62**, 649-671

461 7 V. Branco, J. Canario, A. Holmgren and C. Carvalho, *Toxicol. Appl. Pharmacol.*, 2011, **251**,

462 95-103.

463 8 M. Kunimoto, *Biochem. Biophys. Res. Commun.*, 1994, **204**, 310–317.

464 9 S.-H. Chang, H. J. Lee, B. Kang, K.-N. Yu, A. Minai-Tehrani, S. Lee, S. U. Kim and M.-H.

465 Cho, *J. Toxicol. Sci.*, 2013, **38**, 823–31.

466 10 E. M. Faustman, R. A. Ponce, Y. C. Ou, M. A. C. Mendoza, T. Lewandowski and T.

467 Kavanagh, *Environ. Heal. Perspect.*, 2002, **110**, 859-864.

468 11 J. L. Luque-Garcia, R. Sanchez-Diaz, I. Lopez-Heras, P. Martin and C. Camara, *Trends Anal.*

469 *Chem.*, 2013, **43**, 254–268.

470 12 S. E. Ong and M. A. Mann, *Nat. Protoc.*, 2006, **1**, 2650-2660

471 13 S. Cuello, L. Goya, Y. Madrid, S. Campuzano, M. Pedrero, L. Bravo, C. Camara and S.

472 Ramos, *Food Chem. Toxicol.*, 2010, **48**, 1405–1411.

473 14 E. Fonfria, E. Dare, M. Benelli, C. Sunol and S. Ceccatelli, *Eur. J. Neurosci.*, 2013, **16**, 2013-

474 2016

475 15 S. Cuello, P. Ximenez-Embun, I. Ruppen, H. B. Schonthaler, K. Ashman, Y. Madrid, J. L.

476 Luque-Garcia and C. Camara, *Analyst*, 2012, **137**, 5302-5311.

477 16 S. Elmore, *Toxicol. Pathol.*, 2007, **35**, 495–516.

478 17 S. Cuello, S. Ramos, Y. Madrid, J. L. Luque-Garcia and C. Cámara, *Anal. Bioanal. Chem*,

479 2012, **404**, 315-324.

480   18   Q. Liao, F. Ozawa, H. Friess, A. Zimmermann, S. Takayama, J. C. Reed, J. Kleeff and M. W.

481   Büchler, *FEBS Lett.*, 2001, **503**, 151–157.

482   19   M. MacFarlane and A. C. Williams, *EMBO Report,* 2004, **5**, 674-678.

483   20   M. Vogler, *Cell Death Differ.*, 2012, **19**, 67–74.

484   21   C. Wójcik, *J.Cell Mol. Med.,* 2002, **6**, 25-48.

485   22   L. Grau, J. L. Luque-Garcia, P. Gonzalez-Peramato, D. Theodorescu, J. Palou, J. M.

486   Fernandez-Gomez and M. Sanchez-Carbayo, *Plos One,* 2013, **8**, DOI: 10.1371/journal.pone.0053328.

487   23   A. B. Parrish, C. D. Freel and S. Kombluth, *Cold Spring Harb. Perspect. Biol.*, 2013, **5**, DOI:

488   10.1101/cshperspect.a008672

489   24   Z. Jin, Y. Li, R. Pitti, D. Lawrence, V. C. Pham, J. R. Lill and A. Ashkenazi, *Cell,* 2009, **127**,

490   721-735.

491   25   T. Schmaler and W. Dubiel, *Subcell Biochem.*, 2010, **54**, 57–68.

492   26   D. Lei, F. Li, S. Huabo, J. Liu, N. Wei and X. Wang, *Plos One,* 2013, **8**, DOI:

493   10.1371/journal.pone.0067793

494   27   K. Sokolowski, A. Falluel-Morel, X. Zhou and E. DiCicco-Bloom, *Neurotoxicology*, 2011, **32**,

495   535-544.

496   28   Y. Furukawa, S. Iwase, Y. Terui, J. Kikuchi, T. Sakai, M. Nakamura, S. Kitagawa and M.

497   Kitagawa, *J. Biol. Chem.*, 1996, **271**, 28469–28477.

498   29   L. Zhou, X. Cai, X. Han, N. Xu and D. C. Chang, *Cell Biol. Int.*, 2014, **38**, 737–746.

499   30   P. K. Politis, S. Akrivou, C. Hurel, O. Papadodima and R. Matsas, *FEBS Lett.*, 2008, **582**,

500   741–748.

501   31   N. Georgopoulou, C. Hurel, P. K. Politis, M. Gaitanou, R. Matsas and D. Thomaidou, *J. Biol.*

502   *Chem.*, 2006, **281**, 33606–33620.

503   32   B. M. Filippi, P. de los Heros, Y. Mehellou, I. Navratilova, R. Gourlay, M. Deak, L. Plater, R.

504   Toth, E. Zeqiraj and D. R. Alessi, *EMBO J.*, 2011, **30**, 1730–1741.

505   33   I. Dan, S. E. Ong, N. M. Watanabe, B. Blagoev, M. M. Nielsen, E. Kajikawa, T. Z.

506   Kristiansen, M. Mann and A. Pandey, *J. Biol. Chem.*, 2002, **277**, 5929–5939.

507   34   Z. Shi, S. Jiao, Z. Zhang, M. Ma, Z. Zhang, C. Chen, K. Wang, H. Wang, W. Wang, L. Zhang,

508   Y. Zhao and Z. Zhou, *Structure,* 2013, **21**, 449-461.

509   35   B. D. Gelbman, A. Heguy, T. P. O´Connor, J. Zabner and R. G. Crystal, *Respir. Res.*, 2007, **8**,

510   10

511   36   D. Orzaez, A. J. de Jong and E. J. Woltering, *Plant Mol. Biol.*, 2001, **46**, 459–468.

512   37   E. Patel and M. Reynold, *Toxicol. Lett,* 2013, **222**, 265-272.

513   38   D. Martinvalet, D. M. Dykxhoorn, R. Ferrini and J. Lieberman, *Cell*, 2008, **133**, 681-692.

514   39   G. Huang, Y. Chen, H. Lu and X. Cao, *Cell Death Differ.*, 2007, **14**, 327–337.

515   40   S. Suhane, H. Kanzaki, V. Arumugaswami, R. Murali and V. K. Ramanujan, *Biol. Open*, 2013,

516   **14**, 295–305.

517   41   E. Röth, N. Marczin, B. Balatonyi, S. Ghosh, V. Kovács, N. Alotti, B. Borsiczky and B. Gasz,

518   *Exp. Clin. Cardiol.*, 2011, **16**, 92–96.

519   42   T. Wada and J. Penninger, *Oncogene*, 2004, **23**, 2838-2849.

520   43   E. S. J. Arner and A. Holmgren, *Eur. J. Biochem.*, 2000, **267**, 6102–6109.

521   44   S. Singh, C. Brocker, V. Koppaka, C. Ying, B. Jackson, A. Matsumoto, D. C. Thompson and

522   V. Vasiliou, *Free Radic.*, 2013, **56**, 89-101.

523   45   T. Guida, G. Salvatore, P. Faviana, R. Giannini, G. Garcia-Rostan, L. Provitera, F. Basolo, A.

524   Fusco, F. Carlomagno and M. Santoro, *J. Clin. Endocrinol. Metab.*, 2005, **90**, 4703–4709.

525   46   M. Das, S. Singh, S. Pradhan and G. Narayan, *Mol. Biol. Int.*, 2014, DOI:

526   10.1155/2014/574850.

527   47   R. Ohara, K. Hata, N. Yasuhara, R. Mehmood, Y. Yoneda, M. Nakagawa and T. Yamashita,

528   *Biochem. Biophys. Res. Commun.*, 2011, **405**, 697–702.

529   48   S. Kurklinsky, J. Chen and M. A. McNiven, *J. Neurochem.*, 2011, **177**, 48–60.

530   49   E. Torre, M. A. McNiven and R. Urrutia, *J. Biol. Chem.*, 1994, **269**, 32411–32417.

531   50   G. Paglini, P. Kunda, S. Quiroga, K. Kosik and A. Caceres, *J. Cell Biol.*, 1998, **143**, 443–455.

532   51   E. Lu, P. Fox, M. Lakonishok, M. W. Davidson and V. I. Gelfand, *Curr. Biol.*, 2013, **23**,

533   1018–1023.

534   52   J. C. Pendergrass, B. E. Haley, M. J. Vimy, S. A. Winfield and F. L. Lorscheider,

535   *Neurotoxicology,* 1997, **18**, 315-324.

536   53   T. J. Lightfoot, C. F. Skibola, E. V Willett, D. R. Skibola, J. M. Allan, F. Coppede, P. J.

537   Adamson, G. J. Morgan, E. Roman and M. T. Smith, *Cancer Epidemiol. Biomarkers Prev.*, 2005, **14**,

538   2999-3003.

539   54   L. B. Bailey and J. F. Gregory, *J. Nutr.*, 1999, **129**, 779-782.

540   55   J. Y. Fowdar, M. V Lason, A. L. Szvetko, R. A. Lea and L. R. Griffiths, *Int. J. Hypertens.*,

541   2012, DOI: 10.1155/2012/190923.

542   56   M. Waly, H. Olteanu, R. Banerjee, S.-W. Choi, J. B. Mason, B. S. Parker, S. Sukumar, S.

543   Shim, a Sharma, J. M. Benzecry, V. Power-Charnitsky and R. C. Deth, *Mol. Psychiatry.*, 2004, **9**, 358–

544   370.

545   57   M. J. Shipton and J. Thachil, 2015, *Clin.Med.*, 2015, **15**, 145-150.

546   58   D. G. Weir and J. M. Scott, *Br. Med. Bull*, 1999, **55**, 669-682.

547   59   C. M. Gallagher and J. R. Meliker, *Sci. Total Env.*, 2011, **409**, 1399-1405.

548   60   A. Boldyrev, E. Bryushkova, A. Mashkina and E. Vladychenskaya, *Aging Sci*, 2013, **6**, 29-36.

549   61   E. Ziemińska, A. Stafiej and J. W. Łazarewicz, *Neurochem. Int*, 2003, **43**, 481-492.

550   62   B. Ahlrot-Westerlund, *Heavy Metal Bull.*, 1995, **3**, 11-12.

551   63   J. L. Luque-Garcia, P. Cabezas-Sanchez and C. Camara, *Trends Anal. Chem. 30*, 2011, **30**,

552   703–716.

553

554

555

556

557

558

559

560

561

562

563

564

565

566

567

568

569

Figure Captions

571 **Fig. 1** Cytotoxicity, mercury uptake and morphological changes induced by MeHg exposure. **a**

572 Viability of Neuro-2a cells exposed to different concentrations (0.5, 2 and 5 mg L^{-1}) of MeHg at

573 various exposure times (n = 10) While the viability of cells exposed to 0.5 mg L^{-1} MeHg was not

574 affected at any of the exposure times tested, 5 mg L^{-1} MeHg caused a decrease on the cell viability

575 close to 100% even after 6 h of exposure. We selected 2 mg L^{-1} and 8 h exposure for further

576 experiment to evaluate the effect of MeHg on Neuro-2a cells without drastically compromising the cell

577 viability. **b** Morphological changes induced after MeHg exposure visualized by fluorescence

578 microscopy after staining with phalloidin-FITC and DAPI (n = 3). Exposure to MeHg markedly

579 disrupted the structural integrity of neurites. **c** Determination of the total amount of MeHg internalized

580 by the cells by atomic fluorescence spectroscopy (AFS) (n = 4). Only 10% of the total MeHg added

581 were actually found inside the cells.

582

583 **Fig. 2** SILAC results. **a** General scheme of the SILAC procedure. **b** Distribution of the SILAC ratios

584 for the identified proteins. Most quantified proteins presented a SILAC ratio close to 1, as expected for

585 a 1:1 mixture. **c** Functional annotation of the 125 altered proteins upon MeHg exposure obtained from

586 the gene ontology GO consortium website. Major molecular and cellular functions altered included cell

587 death (CD), RNA post-transcriptional modification (PT), protein synthesis (P), cellular assembly and

588 organization (AO), and cell cycle (CC).

589

590 **Fig. 3** Schematic representation of the methylation cycle. Vitamin B12 (B12); glutathione S-transferase

591 P (GSTP1); methionine synthase (MTR); methylenetetrahydrofolate dehydrogenase (MTHFD1);

592 methylenetetrahydrofolate reductase (MTHFR); S-adenosylmethionine (SAM); S-

593 adenosylhomocystine (SAH); tetrahydrofolate (THF).

594

595 **Fig. 4** Evaluation of the levels of MTHFD1 and MTR in Neuro-2a cells exposed to different

596 concentration of MeHg by Western Blot analysis (n = 3). The expression of MTHFD1 and MTR

597 decreased significantly with increasing concentrations of MeHg. GAPDH was used as loading control.

598

599   **Fig. 5** siRNA-mediated gene knock-down of MTHFD1. **a** Immnunoblotting of Control vs. MTHFD1

600   knock-down (KD) that shows the suitability of the transfection (n = 3). **b** Comparison of viability

601   between Neuro-2a cells transfected with 30 pmols of siRNA-MTHFD1 and cells exposed to 2 mg L^{-1}

602   of MeHg for 8 h (n = 10)**.** MTHFD1 knock-down affected the viability of Neuro-2a cells, although the

603   decrease in cell viability was more pronounced in cells exposed to MeHg.

604

605   **Fig. 6** Effect of high levels of vitamin B12 supplementation to MeHg-exposed Neuro-2a cells (n = 10).

606   Supplementation with vitamin B12 did not ameliorate the decreased in cell viability observed in

607   MeHg-exposed cells.

608

609   **Fig. 7** Comparative effect of MeHg and other heavy metals on the expression of MTHFD1 and MTR (n

610   = 3). The four species highly affect the expression of MTR while the expression of MTHFD1 was

611   significantly different depending on the metallic species tested.

612

613

614

615

616

617

618

619

620

621

622

623

624

625

626

627

628   **Table 1**. Proteins up-regulated in Neuro-2a cells exposed to MeHg

629

Common Name	Accession Number	Protein name	Silac ratio	RSD	Mascot Score
MCM5	112293273	minichromosome maintenance deficient 5, cell division cycle 46	3,71	4,14	131
PIR	51317401	pirin	2,98	4,71	113
ALDH2	6753036	aldehyde dehydrogenase 2, mitochondrial	2,93	12,14	194
CAD	51093867	carbamoyl-phosphate synthetase 2, aspartate transcarbamylase, and dihydroorotase	2,92	11,24	92
CDK1	31542366	cell division cycle 2 homolog A	2,80	1,87	502
MO25	31982582	MO25 protein	2,68	8,85	82
NDUFS3	58037117	NADH dehydrogenase (ubiquinone) Fe-S protein 3	2,65	1,03	238
RPF2	110347519	brix domain containing 1 isoform 1	2,53	10,31	119
BAX	6680770	Bcl2-associated X protein	2,52	12,48	750
PRPF8	115583687	pre-mRNA processing factor 8	2,30	9,28	320

TRXR1	**13569841**	thioredoxin reductase 1 isoform 2	**2,23**	13,31	381
CEND1	**10946620**	cell cycle exit and neuronal differentiation 1	**2,10**	17,11	128
EIF4B	**21704128**	eukaryotic translation initiation factor 4B	**2,05**	16,61	57
DUT	**21281687**	deoxyuridine triphosphatase	**2,00**	15,19	408
TRX	**31543902**	thioredoxin	**1,99**	0,98	136
USMG5	**77404294**	upregulated during skeletal muscle growth 5	**1,91**	4,96	169
CUL3	**7710014**	cullin 3	**1,88**	12,53	98
NXF1	**31980798**	nuclear RNA export factor 1	**1,85**	13,70	122
AP1B1	**88853578**	adaptor protein complex AP-1, beta 1 subunit	**1,85**	15,07	444
MCM2	**6678826**	minichromosome maintenance deficient 2 mitotin	**1,85**	16,25	118
PSMB2	**31981327**	proteasome (prosome, macropain) subunit, beta type 2	**1,83**	14,80	555
PDXP	**47059486**	pyridoxal phosphate phosphatase	**1,80**	12,33	272
NAP1L4	**6679012**	nucleosome assembly protein 1-like 4	**1,79**	12,67	256

RPS28	**21426821**	ribosomal protein S28	**1,76**	10,93	131
EIF2S3X	**6753738**	eukaryotic translation initiation factor 2, subunit 3, structural gene X-linked	**1,75**	17,77	101
SORD	**22128627**	sorbitol dehydrogenase	**1,73**	12,27	109
EIF2S2	**14149756**	eukaryotic translation initiation factor 2, subunit 2 (beta)	**1,71**	8,30	149
PAICS	**13385434**	phosphoribosylaminoimidazole carboxylase, phosphoribosylaminoimidazole succinocarboxamide synthetase	**1,69**	19,50	258
CKAP5	**66955862**	cytoskeleton associated protein 5	**1,67**	18,10	238
PRDX5	**6755114**	peroxiredoxin 5 precursor	**1,67**	0,45	169
LMNA	**50355692**	lamin A isoform A	**1,67**	17,15	642
ENO1	**12963491**	enolase 1, alpha non-neuron	**1,65**	15,15	141
RSL24D1	**38348464**	ribosomal protein L24-like	**1,62**	6,94	280

PLCXD3	**28893495**	phosphatidylinositol-specific phospholipase C, X domain containing 3	**1,62**	6,82	193
IPO4	**19745156**	RANBP4	**1,61**	9,44	154
EIF3I	**9055370**	eukaryotic translation initiation factor 3, subunit 2 (beta)	**1,59**	17,18	621
U2AF1	**17530980**	U2 small nuclear ribonucleoprotein auxiliary factor (U2AF) 1	**1,59**	17,21	96
ALG2	**31560366**	alpha-1,3-mannosyltransferase ALG2	**1,58**	9,45	92
PSMD11	**134053905**	proteasome 26S non-ATPase subunit 11	**1,58**	10,38	425
FAM49B	**21450053**	hypothetical protein LOC223601	**1,58**	12,93	238
TIMM23	**12025536**	translocase of inner mitochondrial membrane 23 homolog	**1,55**	18,91	184
ATAD1	**31560168**	ATPase family, AAA domain containing 1	**1,53**	8,15	378
CNOT1	**94383743**	PREDICTED: CCR4-NOT transcription complex, subunit 1 isoform 2	**1,53**	0,90	137

VAMP3	6678553	vesicle-associated membrane protein 3	1,51	2,20	193
TSTA3	13654268	tissue specific transplantation antigen P35B	1,51	11,51	291
DNAJC8	27369493	DnaJ (Hsp40) homolog, subfamily C, member 8	1,51	2,81	88
PRPF19	19527358	nuclear matrix protein SNEV	1,51	9,57	115
ITGB1	45504394	integrin beta 1 (fibronectin receptor beta)	1,50	11,37	152

630

631

632

633

634

635

636

637

638

639

640

641

642

643

644

26

645   **Table 2**. Proteins down-regulated in Neuro-2a cells exposed to MeHg

Common Name	Accession Number	Protein name	Silac ratio	RSD	Mascot Score
KIF5C	45433560	kinesin family member 5C	-18,73	8,92	139
RAB1B	21313162	RAB1B, member RAS oncogene family	-15,31	12,26	1199
NSF	31543349	N-ethylmaleimide sensitive fusion protein	-8,34	12,52	265
PCM1	13540494	pericentriolar material 1	-8,02	10,22	96
SMARCA4	76253779	SWI/SNF related, matrix associated, actin dependent regulator of chromatin, subfamily a, member 4	-7,95	10,04	156
PICALM	32567788	phosphatidylinositol-binding clathrin assembly protein	-7,70	12,36	287
TPPP3	13385968	hypothetical protein LOC67971	-7,20	16,97	90
TCEB1	21312712	transcription elongation factor B (SIII), polypeptide 1	-5,94	5,98	142
ACSL4	46518528	acyl-CoA synthetase long-chain family member 4 isoform 1	-5,76	14,62	105
-	149262716	PREDICTED: similar to hCG1813078	-5,72	14,82	117
ATP5L	31980744	ATP synthase, H+ transporting, mitochondrial F0 complex, subunit G	-4,93	9,37	232
NT5C3B	31980891	5'-nucleotidase, cytosolic III-like	-4,73	4,95	92

TUBB2B	21746161	tubulin, beta	-4,48	8,62	3658
PGM2	31980726	phosphoglucomutase 2	-4,48	6,41	114
CBR3	27413160	carbonyl reductase 3	-4,34	6,04	38
CTTN	75677414	cortactin	-3,84	5,83	51
COP9	7242142	COP9 (constitutive photomorphogenic) homolog, subunit 7a	-3,45	5,81	242
DDX39	38372907	DEAD (Asp-Glu-Ala-Asp) box polypeptide 39	-3,30	17,44	297
NDUFB10	58037109	NADH dehydrogenase (ubiquinone) 1 beta subcomplex, 10	-2,83	2,15	433
ATP5J2	10181184	ATP synthase, H+ transporting, mitochondrial F0 complex, subunit f, isoform 2	-2,73	11,28	70
PSMA4	6755196	proteasome (prosome, macropain) subunit, alpha type 4	-2,56	16,41	230
TMPO	121949765	thymopoietin isoform epsilon	-2,51	2,00	313
KIF11	45476577	kinesin family member 11	-2,41	7,51	87
RQCD1	10946722	rcd1 (required for cell differentiation) homolog 1	-2,33	10,46	103
THOP1	31981237	thimet oligopeptidase 1	-2,29	3,82	376
IPO	112734861	importin	-2,24	13,83	172
-	149252028	PREDICTED: hypothetical protein	-2,17	0,65	231

SRSF6	31543689	arginine/serine-rich splicing factor 6	**-2,14**	10,06	109
ATAD3	30725845	AAA-ATPase TOB3	**-2,09**	17,44	141
PDLIM3	7948997	PDZ and LIM domain 3	**-2,07**	10,83	201
ARPC3	9790141	actin related protein 2/3 complex, subunit 3	**-2,05**	19,19	65
COX5A	112181182	cytochrome c oxidase, subunit Va	**-2,02**	13,30	141
CHCHD3	149254953	PREDICTED: hypothetical protein	**-1,99**	12,73	228
HNRNPC	8393544	heterogeneous nuclear ribonucleoprotein C	**-1,98**	6,39	336
SLC25A1	23943838	solute carrier family 25, member 1	**-1,96**	13,33	82
COPE	10946972	epsilon subunit of coatomer protein complex	**-1,94**	10,74	353
TRNT1	33859692	tRNA nucleotidyl transferase, CCA-adding, 1	**-1,92**	5,80	187
MYEF2	27819594	myelin basic protein expression factor 2, repressor	**-1,91**	3,53	78
KRAS	84370270	c-K-ras2 protein	**-1,91**	0,65	137
PFKL	31560653	phosphofructokinase, liver, B-type	**-1,89**	12,56	88
RPF2	110347521	brix domain containing 1 isoform 2	**-1,89**	10,02	179
HNRNPR	33859724	heterogeneous nuclear ribonucleoprotein R	**-1,86**	18,16	226
BDH1	31982169	3-hydroxybutyrate dehydrogenase, type 1	**-1,83**	0,56	132
TUBA1C	6678469	tubulin, alpha 1C	**-1,83**	14,45	507
TNPO1	115385966	transportin 1 isoform 2	**-1,81**	13,62	389

BAG3	115270960	Bcl2-associated athanogene 3	**-1,81**	15,06	384
H1FX	38348566	H1 histone family, member X	**-1,81**	16,15	207
RBM25	124430762	RNA binding motif protein 25	**-1,80**	9,76	72
BCAT1	66792792	branched chain aminotransferase 1, cytosolic isoform 1	**-1,78**	3,61	257
-	149249564	PREDICTED: hypothetical protein isoform 1	**-1,77**	14,21	224
GST	6754086	glutathione S-transferase	**-1,74**	15,07	207
PPP2R4	31981677	protein phosphatase 2A, regulatory subunit B (PR 53)	**-1,73**	0,51	200
SRRT	13937395	arsenate resistance protein 2	**-1,73**	13,47	132
MSN	70778915	moesin	**-1,72**	4,91	141
-	94390383	PREDICTED: similar to La ribonucleoprotein domain family, member 1	**-1,72**	17,54	105
RRM1	31982026	ribonucleotide reductase M1	**-1,71**	16,03	175
MEST	6678866	mesoderm specific transcript	**-1,70**	3,33	259
SNCB	15809030	synuclein, beta	**-1,69**	7,68	208
DYN	134288917	dynein	**-1,68**	18,65	733
MTHFD1	31559887	methylenetetrahydrofolate dehydrogenase (NADP+ dependent) 1	**-1,67**	18,63	317

AP2A1	6671561	adaptor protein complex AP-2, alpha 1 subunit isoform a	**-1,66**	6,45	132
NASP	125490378	nuclear autoantigenic sperm protein isoform 2	**-1,65**	14,21	60
RBMX	6755296	RNA binding motif protein, X-linked	**-1,64**	9,19	221
BCL2A1	24496776	BCL2-associated transcription factor 1 isoform 2	**-1,64**	18,50	82
-	149265144	PREDICTED: filamin B, beta	**-1,62**	14,83	422
STMN1	9789995	stathmin 1	**-1,59**	17,20	129
SMC1A	9790237	SMC1 structural maintenance of chromosomes 1-like 1	**-1,58**	14,20	129
DDX18	31981163	DEAD (Asp-Glu-Ala-Asp) box polypeptide 18	**-1,58**	19,13	80
PSMD5	134053913	proteasome 26S non-ATPase subunit 5	**-1,56**	16,01	98
SLC3A2	31560670	solute carrier family 3 (activators of dibasic and neutral amino acid transport), member 2	**-1,55**	13,75	178
TRA2B	6677975	splicing factor, arginine/serine-rich 10	**-1,55**	0,74	235
LOC433762	149253163	PREDICTED: hypothetical protein	**-1,54**	13,95	444
DDX21	72384374	DEAD (Asp-Glu-Ala-Asp) box polypeptide 21	**-1,53**	1,82	701
PRPH	7305413	peripherin	**-1,52**	17,67	1706
SNX2	13385878	sorting nexin 2	**-1,51**	18,33	73
TARS	27229277	threonyl-tRNA synthetase	**-1,51**	10,43	319

| EIF4A3	20149756	eukaryotic translation initiation factor 4A, isoform 3	-1,50	1,16	389

646

647

Figure 1
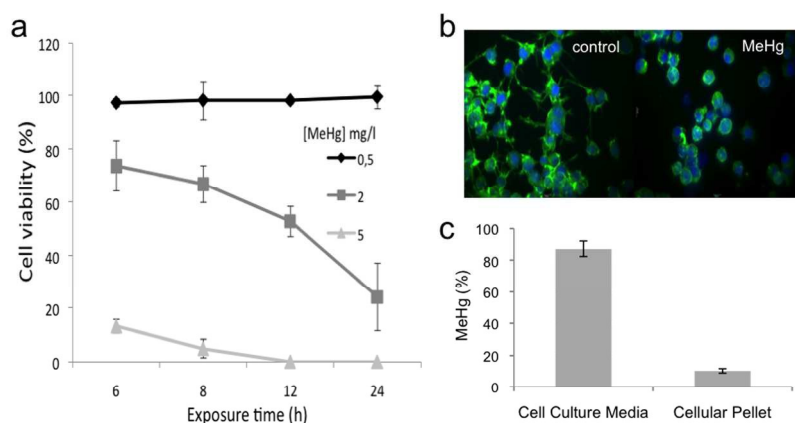
Cytotoxicity, mercury uptake and morphological changes induced by MeHg exposure. a Viability of Neuro-2a cells exposed to different concentrations of MeHg at various exposure times.
While the viability of cells exposed to 0.5 mg L-1 MeHg was not affected at any of the exposure times tested, 5 mg L-1 MeHg caused a decrease on the cell viability close to 100% even after 6 h of exposure. We selected 2 mg L-1 and 8 h exposure for further experiment to evaluate the effect of MeHg on Neuro-2a cells without drastically compromising the cell viability. b Morphological changes induced after MeHg exposure visualized by fluorescence microscopy after staining with phalloidin-FITC and DAPI. Exposure to MeHg markedly disrupted the structural integrity of neurites. c Determination of the total amount of MeHg internalized by the cells by atomic fluorescence spectroscopy (AFS). Only 10% of the total MeHg added were actually found inside the cells.

199x199mm (300 x 300 DPI)

Figure 2
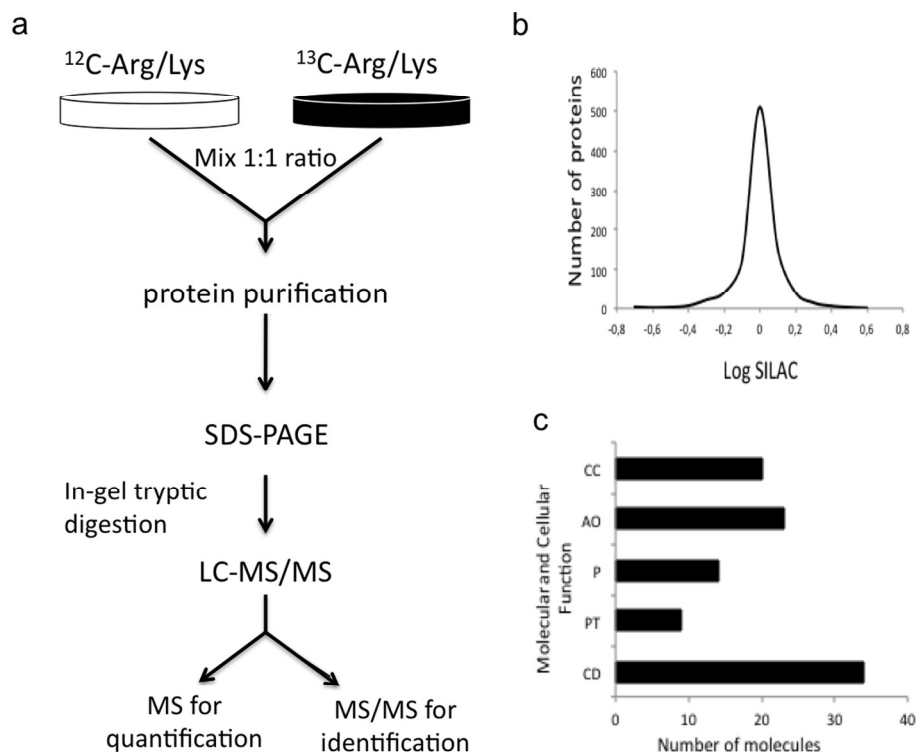
SILAC results. a General scheme of the SILAC procedure. b Distribution of the SILAC ratios for the identified proteins. Most quantified proteins presented a SILAC ratio close to 1, as expected for a 1:1 mixture. c Functional annotation of the 125 altered proteins upon MeHg exposure obtained from the gene ontology GO consortium website. Major molecular and cellular functions altered included cell death (CD), RNA post-transcriptional modification (PT), protein synthesis (P), cellular assembly and organization (AO), and cell cycle (CC).
203x199mm (300 x 300 DPI)

Figure 3
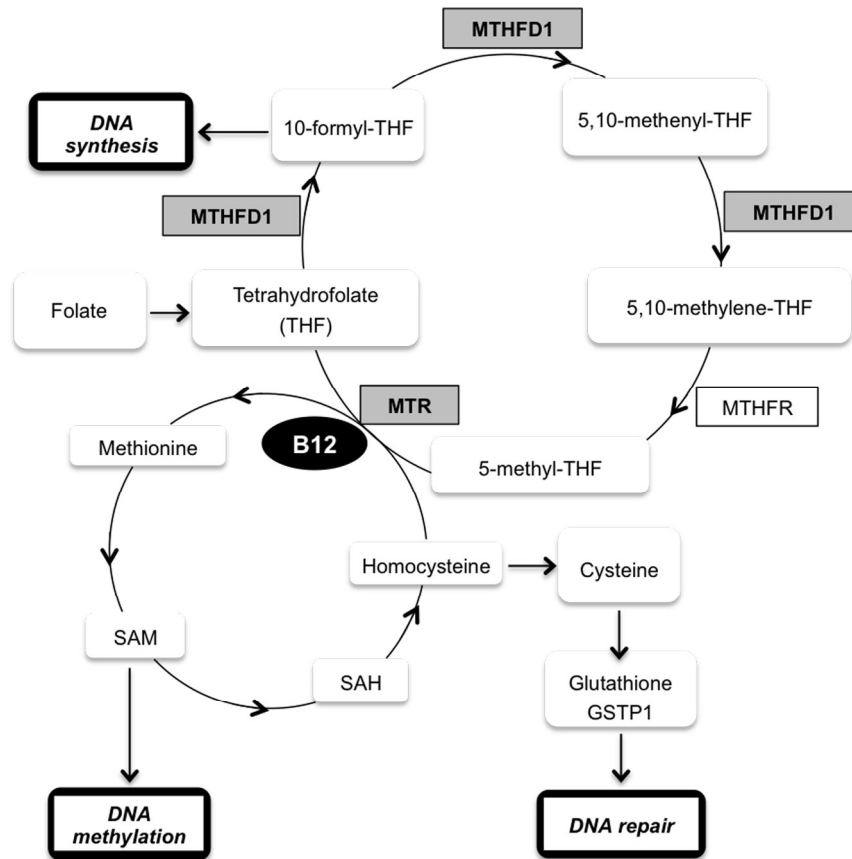
Schematic representation of the methylation cycle
174x199mm (300 x 300 DPI)

Figure 4
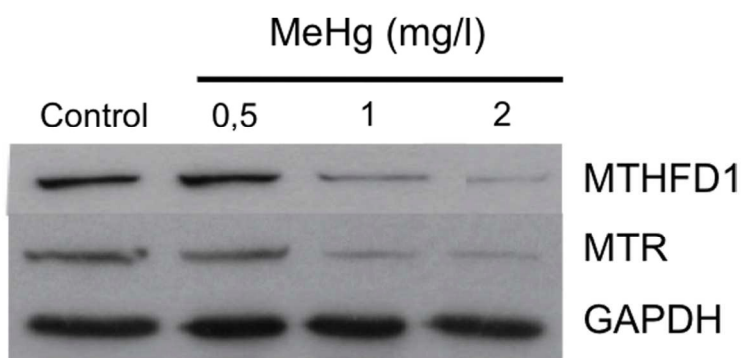
Evaluation of the levels of MTHFD1 and MTR in Neuro-2a cells exposed to different concentration of MeHg by Western Blot analysis. The expression of MTHFD1 and MTR decreased significantly with increasing concentrations of MeHg. GAPDH was used as loading control.
119x150mm (300 x 300 DPI)

Figure 5
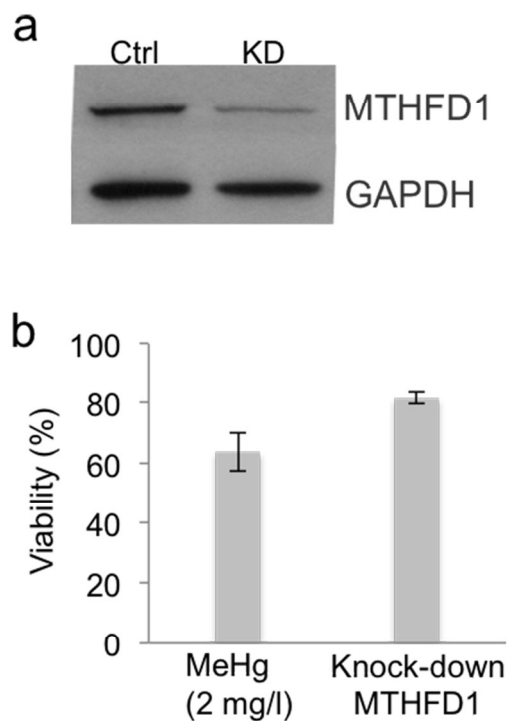
siRNA-mediated gene knock-down of MTHFD1. a Immnunoblotting of Control vs. MTHFD1 knock-down (KD) that shows the suitability of the transfection. b Comparison of viability between Neuro-2a cells transfected with 30 pmols of siRNA-MTHFD1 and cells exposed to 2 mg L-1 of MeHg for 8 h. MTHFD1 knock-down affected the viability of Neuro-2a cells, although the decrease in cell viability was more pronounced in cells exposed to MeHg.
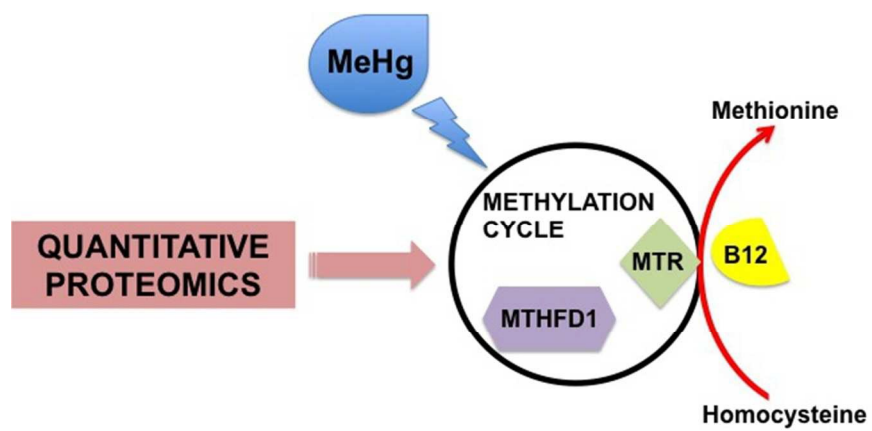99x160mm (300 x 300 DPI)

Figure 6
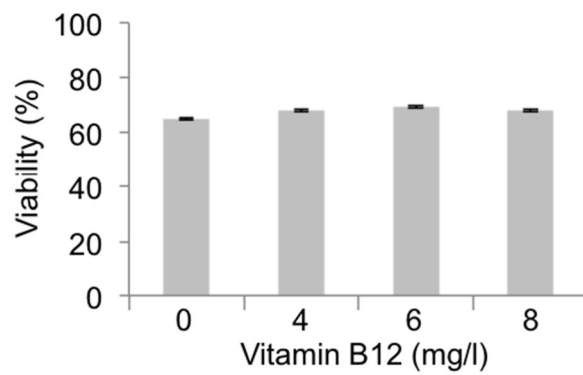
Effect of high levels of vitamin B12 supplementation to MeHg-exposed Neuro-2a cells. Supplementation with vitamin B12 did not ameliorate the decreased in cell viability observed in MeHg-exposed cells.
140x150mm (300 x 300 DPI)

Figure 7
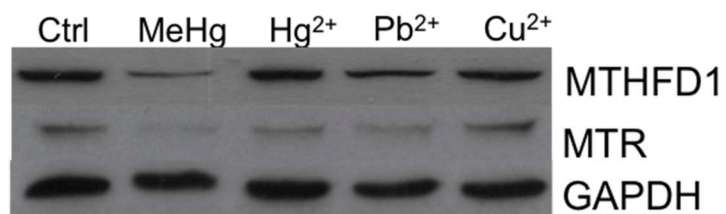
Comparative effect of MeHg and other heavy metals on the expression of MTHFD1 and MTR. The four species highly affect the expression of MTR while the expression of MTHFD1 was significantly different depending on the metallic species tested.
119x150mm (300 x 300 DPI)

263x140mm (72 x 72 DPI)